# Hyperfine and Nuclear Quadrupole Couplings of the Coordinated Nitrogen of Oxovanadium(IV) Phthalocyanines Studied by Electron Spin-Echo Envelope Modulation Spectroscopy

**Kouichi Fukui,* Hiroaki Ohya-Nishiguchi, Hitoshi Kamada, Masamoto Iwaizumi,† and Yuanzhi Xu††**

Institute for Life Support Technology, Yamagata Technopolis Foundation, Matuei 2-2-1, Yamagata 990-2473

†Institute for Chemical Reaction Science, Tohoku University, Katahira 2-2-1, Aoba-Ku, Sendai 980-8577

††Department of Chemistry, Zhejiang University, Hangzhou, 310027, P. R. China

(Received May 12, 1998)

Electron spin-echo envelope modulation (ESEEM) measurements were made for three substituted oxovanadium(IV) phthalocyanines ([VO(tcpc)], [VO(tbpc)], and [VO(tapc)]), where the phthalocyanine rings are modified with four carboxyl, *t*-butyl, and amino groups, respectively. The $^{14}$N hyperfine coupling (HFC) and nuclear quadrupole coupling (NQC) tensors of the phthalocyanine isoindole nitrogens were determined by computer simulations of orientationally selected ESEEM spectra. The HFC tensors of these three complexes were found to be almost identical, and no appreciable effects from the substituents were detected. The isotropic HFC constants, as determined by the simulations, are $|A_{iso}|$ = 7.08, 7.08, and 7.05 MHz for [VO(tcpc)], [VO(tbpc)], and [VO(tapc)], respectively. The NQC constants were also found to be very similar to one another: $e^2qQ/h$ = 2.2, 2.1, and 2.0 MHz for [VO(tcpc)], [VO(tbpc)], and [VO(tapc)], respectively. However, the simulations revealed a difference in the orientation of the NQC unique axis, where the unique axis is parallel to the V–N bond in [VO(tcpc)] and [VO(tbpc)], whereas this axis is perpendicular to the V–N bond within the phthalocyanine plane in [VO(tapc)]. An analysis of the NQC parameters based on the Townes-Dailey model indicates an increase in the electron population of the nitrogen $\pi$ orbital in [VO(tapc)], which is consistent with the expected effects of the amino group.

Electron-spin echo envelope modulation (ESEEM) spectroscopy is a powerful method to investigate the environments of paramagnetic centers, probing weak couplings (typically$\leq$10 MHz) between an unpaired electron spin and nearby nuclear spins.[1,2] This spectroscopy has been applied to a number of oxovanadium(IV) complexes, and the hyperfine coupling (HFC) due to $^{14}$N nuclei coordinated directly to $VO^{2+}$ ion has been investigated. Through these studies, a useful correlation has been found to exist between the magnitude of HFC and the type of nitrogen.[3,4] The correlation can be summarized in terms of the isotropic HFC parameter ($A_{iso}$) as (1) $|A_{iso}| \approx 5$ MHz for $sp^3$-hybrid amine nitrogens, (2) $\approx$ 6—7 MHz for $sp^2$-hybrid imine nitrogens, and (3) $\approx$ 7.5 MHz for the sp-hybrid isothiocyanate nitrogen. The $sp^2$-hybrid imine nitrogens may be further divided into two subclasses as (2a) $|A_{iso}| \approx$ 6—6.5 MHz for Schiff-base nitrogens, pyridines and imidazoles,[5,6] and (2b) $\approx$ 7 MHz for porphyrin pyrrole nitrogens.[7] Phthalocyanines also have $sp^2$-hybrid nitrogens (isoindole nitrogens) capable of coordinating to metal ions. The HFC of this type of nitrogens attracts interest because of its close relation to porphyrin nitrogens. However, to the best of our knowledge, oxovanadium(IV) phthalocyanines have not been studied by ESEEM or electron-nuclear double resonance (ENDOR) spectroscopy, and thus the HFC parameters of the phthalocyanine nitrogen are not known.

In addition to the close relation to biologically relevant porphyrins and chlorophills, phthalocyanines themselves have been receiving great attention owing to their versatile characteristics, such as usefulness as dyes and pigments,[8] photocatalytic activities,[9] and solid-state conductivity.[10] Several substituted phthalocyanines have been synthesized with the aim to improve these characterisctics.[9,11,12] Substituents are expected to modify the solubility, redox potential, electronic properties, crystal packing, and other chemical and physical properties. Substituents will also affect the HFC and nuclear quadrupole coupling (NQC) of the phthalocyanine isoindole nitrogen, which simultaneously alter the ESEEM spectral properties of metal phthalocyanines. It is therefore interesting to examine whether such substituent effects are observably large and, if so, how the substituent effects influence the ESEEM spectra.

Here we describe the ESEEM results of three oxovanadium(IV) phthalocyanines: [VO(tcpc)], [VO(tbpc)], and [VO(tapc)] (Scheme 1). We have determined the $^{14}$N HFC and NQC tensors of the phthalocyanine isoindole nitrogens of these complexes by computer simulations of orientationally selected ESEEM spectra. The simulations show that the $^{14}$N HFC parameters of these complexes are almost the same as one another. Furthermore, these HFC parameters are fairly similar to the previously reported $^{14}$N HFC parameters of oxovanadium(IV) porphyrins, [VO(oep)] and

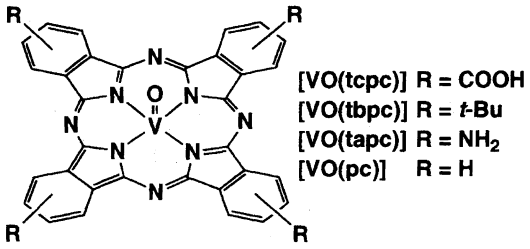


Scheme 1.

[VO(tpp)] ($H_2$oep = 2,3,7,8,12,13,17,18-octaethylporphine, $H_2$tpp = 5,10,15,20-tetraphenylporphine).[7] As for the NQC parameters, on the other hand, we have found a difference in the orientation of the largest magnitude NQC axis (unique axis). We show that this finding can be explained in terms of a change in the electron populations on the nitrogen orbitals due to substituent effects.

## Experimental

**Materials.** The complexes [VO(tcpc)], [VO(tbpc)], and [VO(tapc)] were prepared as previously reported.[13,14] We also investigated the non-substituted complex [VO(pc)]. However, unfortunately, the limited solubility of this complex prevented us from obtaining sufficiently strong electron spin-echo signals. Accordingly, we can not include [VO(pc)] in this study.

**Measurements.** CW EPR and ESEEM measurements were carried out on a JEOL RE-3X EPR spectrometer equipped with a JEOL ES-PX1000 pulse EPR unit. The two-pulse sequence ($\pi/2$–$\tau$–$\pi$–$\tau$–echo) and the three-pulse sequence ($\pi/2$–$\tau$–$\pi/2$–$T$–$\pi/2$–$\tau$–echo) were applied with pulse widths of $t_{\pi/2}$ = 15 ns and $t_{\pi}$ = 30 ns. The repetition rate of the pulse sequence was typically 1 kHz. Microwave pulses were amplified by a Litton M-624 traveling-wave-tube amplifier to a power of a few kilowatts, and introduced to a $TE_{102}$-mode rectangular cavity resonator. Echo signals were accumulated (100—1000 scans, depending on the intensity of the echo signal) on a Tektronix TDS 520B digital oscilloscope, and transferred to a JEOL ESPRIT 330 computer. This procedure was performed typically for 256 times with a 20 ns increase of $\tau$ for two-pulse measurements or $T$ for three-pulse measurements to yield one set of ESEEM time-domain data. The data lost to the instrumental dead time were reconstructed with the linear prediction singular value decomposition (LPSVD)[15] before the time-domain data were converted to a frequency-domain cosine Fourier transform (FT) spectrum. All of the measurements were performed at liquid-nitrogen temperature (77 K) using an Eikohsha liquid-nitrogen dewar vessel.

**Simulations.** Simulations of ESEEM data were carried out on an Apple Power Macintosh 8100 using a home-made program based on the Mims formulas.[16] In the simulation, the HFC **A** and NQC **Q** tensors of each nitrogen were assumed to be coaxial unless specially noted. The coaxial **A** and **Q** tensors are defined in the nitrogen local frame fixed to the nitrogen atom. The orientation of the nitrogen local frame with respect to the molecular frame (**g** tensor frame) is described in terms of the Euler angles ($\alpha$, $\beta$, and $\gamma$; the definition of the Euler angles is given elsewhere).[3] The Euler angles for the four nitrogens were first set at $\alpha$ = 0, 90, 180, 270°, $\beta$ = 0°, and $\gamma$ = 0°, where the $A_z$ ($Q_z$) axis is parallel to the $g_z$ axis and the $A_x$ ($Q_x$) and $A_y$ ($Q_y$) axes are in the $g_{xy}$ plane. In seeking the best fits, we also varied the Euler angles, and it turned out that a variation of $\beta$ is indispensable to achieve the best fits. Thus, the $A_z$ ($Q_z$) axis is not parallel to the $g_z$ axis in the best-fit parameter sets. Nevertheless, we labeled the nitrogen local axis which is nearest to the $g_z$ axis as $z$ ($A_z$ and $Q_z$ axis). As for the nitrogen $x$ and $y$ axes, the axis containing a smaller magnitude HFC component was labeled as $x$, which will be concluded to be parallel to the V–N bond, and the remaining in-plane axis was labeled as $y$. The width of pulse excitation due to the pulse bandwidth and inhomogenious EPR linewidth, which prevents ideal orientation selection, was neglected for simplicity. For $VO^{2+}$ complexes, the separation of the CW EPR $g_{\|}$ and $g_{\perp}$ lines are sufficiently wide compared to the pulse excitation width, so that fairly ideal orientation selection can be made. In fact, although we tentatively performed simulations taking the pulse excitation width into account, the resulting best-fit values were practically identical with those presented in this paper (the difference between them did not exceed the estimated uncertainties).

## Results

**CW EPR Spectroscopy.** The CW EPR spectrum of [VO(tcpc)] in DMF/toluene glass is shown in Fig. 1 as a representative of the oxovanadium(IV) phthalocyanines studied here. All of the three complexes exhibited an axial-type EPR spectrum with the parallel and perpendicular components each split due to the $^{51}$V nuclear spin ($I = 7/2$). The $g$ and $^{51}$V HFC parameters of the oxovanadium(IV) phthalocyanines are listed in Table 1. The oxovanadium(IV) phthalocyanines were previously studied by CW EPR spectroscopy in other glass media, and it was shown that [VO(tcpc)] and [VO(tapc)] exhibit two or more sets of CW EPR signals.[14] For example, two sets of signals were observed from [VO(tapc)] in $C_6H_6$/$CHCl_3$ glass and in DMSO/$CHCl_3$ glass, and some complicatedly overlapping signals were observed from [VO(tcpc)] in DMSO/$CHCl_3$ glass. The appearances of two or more sets of signals were attributed to the coexistence of five-coordinate and six-coordinate species in the glass media.[14] In contrast to these previous observations, we consistently observed only one set of a signal from the oxovanadium(IV) phthalocyanines in DMF/toluene glass, as shown representativlely in Fig. 1. This indicates that only one species is present in DMF/toluene glass, unlike in $C_6H_6$/$CHCl_3$ and

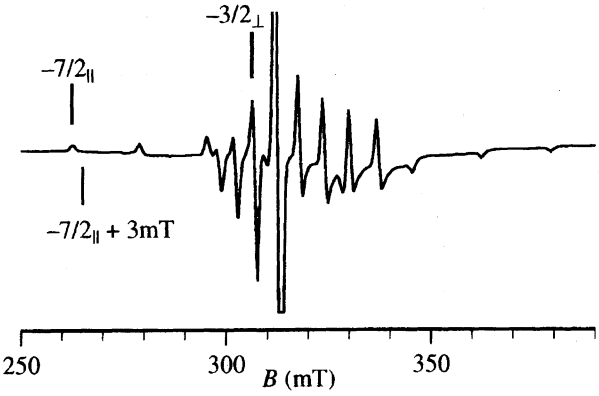


Fig. 1. CW EPR spectrum of [VO(tcpc)] in DMF/toluene (1 : 1 v/v) glass. Conditions: frequency, 8.840 GHz; power, 5 mW; modulation width (100 kHz), 1 mT; temperature, 77 K. The intense "$-1/2_{\|\perp}$" line is truncated for clarity. Representative field positions at which ESEEM measurements were made are indicated as "$-7/2_{\|}$", "$-7/2_{\|}$ +3 mT", and "$-3/2_{\perp}$".

Table 1. CW EPR Parameters of Oxovanadium(IV) Phthalocyanines in DMF/Toluene (1 : 1 v/v) Glass ($T$ = 77 K)

| | $g_\perp$ | $g_\parallel$ | $A_\perp(^{51}\mathrm{V})/10^{-4}$ cm$^{-1}$ | $A_\parallel(^{51}\mathrm{V})/10^{-4}$ cm$^{-1}$ |
|---|---|---|---|---|
| [VO(tcpc)] | 1.982 | 1.970 | 52.0 | 153.7 |
| [VO(tbpc)] | 1.982 | 1.971 | 52.2 | 153.4 |
| [VO(tapc)] | 1.983 | 1.965 | 55.3 | 157.5 |

$DMSO/CHCl_3$ glasses. In order to avoid unnecessary complexity due to the presence of more than one species, we used DMF : toluene glass in ESEEM measurements of the phthalocyanine complexes.

**ESEEM Spectroscopy, General.** Some important field positions employed in ESEEM measurements are indicated in Fig. 1 as "$-7/2_\parallel$", "$-7/2_\parallel+3$ mT", and "$-3/2_\perp$". The position "$-7/2_\parallel$" corresponds to the lowest field parallel line, where the azimuthal quantum number of the $^{51}$V nuclear spin is $m_I(^{51}\mathrm{V}) = -7/2$ ($A(^{51}\mathrm{V}) < 0$ assumed). ESEEM measurements at this line provide "single-crystal-like" spectra,[17] i.e. only those molecules whose $g_z$ axis is parallel to the applied field are selected. The position "$-7/2_\parallel+3$ mT" is an intermediate position upfield of the "$-7/2_\parallel$" line by 3 mT. Measurements at this position provide selective observations of a group of molecules whose $g_z$ axis directs ca. 20° off from the applied field (the angle ca. 20° is estimated from the CW EPR parameters). The position "$-3/2_\perp$" corresponds to the $m_I(^{51}\mathrm{V}) = -3/2$ perpendicular line, and a group of molecules whose $g_z$ axis is perpendicular to the applied field is selectively observed at this position.

All of the three complexes exhibited ESEEM signals attributable to the isoindole $^{14}$N nuclei ($I$ = 1), which is the nitrogen coordinated to the $VO^{2+}$ ion. It seems that the signal due to the bridging nitrogen, which is not coordinated to the $VO^{2+}$ ion, is not observed because of a too small HFC. The observed $^{14}$N ESEEM signals appear over a range of 0—10 MHz. Spectra of this pattern are obtained when HFC exceeds both NQC and the nuclear Zeeman coupling (NZC). In this case, the ESEEM spectra are dominated by the double-quantum (DQ) lines due to the $\Delta M_I = 2$ transitions within the $^{14}$N nuclear spin manifolds.[18] This is in good contrast to the ENDOR spectra, which are usually dominated by single-quantum (SQ) lines ($\Delta M_I = 1$).[19] In the first-order approximation, the DQ lines appear at

$$\nu_{dq\pm} = |A_\zeta| \pm 2\nu(^{14}\mathrm{N}) \quad (1)$$

when magnetic field is applied along the $\zeta$ axis ($\zeta = x, y, z$). Thus, the DQ lines appear as a pair of peaks separated by $4\nu(^{14}\mathrm{N})$ with their center being $|A_\zeta|$. On the other hand, the first-order frequencies of the SQ lines ($\nu_{sq\pm}^{(1)}$ and $\nu_{sq\pm}^{(2)}$) under the same conditions are

$$\nu_{sq\pm}^{(1)} = |A_\zeta|/2 \pm \nu(^{14}\mathrm{N}) + 3|Q_\zeta|/2 \quad (2a)$$

and

$$\nu_{sq\pm}^{(2)} = |A_\zeta|/2 \pm \nu(^{14}\mathrm{N}) - 3|Q_\zeta|/2. \quad (2b)$$

However, according to the Mims formulas,[16] the intensities of the SQ lines are zero when the $g_\zeta$, $A_\zeta$, and $Q_\zeta$ axes are all coincident and the applied field is parallel to this axis. Thus, the SQ lines are only observable when at least one of the axes is misaligned or the applied field is deviated from the tensor axes. In fact, the SQ lines were very weak, or even not observed, in the spectra recorded at "$-7/2_\parallel$", which indicates that the $g_z$, $A_z$, and $Q_z$ axes are roughly colinear in the oxovanadium(IV) phthalocyanines. This situation, however, is somewhat troublesome because the absence of the SQ lines makes it impossible to estimate $|Q_z|$ using Eq. 2. In order to overcome this, we also measured the position "$-7/2_\parallel+3$ mT", where the SQ lines would gain intensities because of a slight deviation of the applied field and, on the other hand, the frequencies of the SQ lines would not be very different from those at the point "$-7/2_\parallel$".

Besides these fundamental lines (SQ and DQ lines), ESEEM spectra can exhibit multinuclear combination lines, which appear at the sum and difference frequencies of some (not all) pairs of fundamental lines. This type of combination occurs because of the presence of two or more nuclear spins interacting with the same electron spin. Since the oxovanadium(IV) phthalocyanines have four nitrogens coordinated to the $VO^{2+}$ ion, this type of combination can be observed. Furthermore, two-pulse spectra can exhibit another type of "sum and difference" combination, which appears even when only one nuclear spin is interacting with an electron spin. Quite interestingly, the time-domain echo modulations due to these "sum and difference" combinations are often in counter phase, so that these combination lines often appear as negative-amplitude peaks in the cosine FT spectra.[18] Important "sum and difference" combinations are as follows: $\nu_{dd+} = \nu_{dq+} + \nu_{dq-} \approx 2|A_\zeta|$, $\nu_{dd-} = \nu_{dq+} - \nu_{dq-} \approx 4\nu(^{14}\mathrm{N})$, and $\nu_{ss+} = \nu_{sq\pm}^{(1)} + \nu_{sq\mp}^{(2)} \approx |A_\zeta|$.[17]

**ESEEM Spectroscopy, [VO(tcpc)].** Figure 2 shows five selected ESEEM spectra of [VO(tcpc)]; the three-pulse spectra recorded at the positions "$-7/2_\parallel$", "$-7/2_\parallel+3$ mT" and "$-3/2_\perp$", and the two-pulse spectra recorded at "$-7/2_\parallel$" and "$-3/2_\perp$". The peak appearing at the $^1$H Larmor frequency ($\nu(^1\mathrm{H}) = 11.0$ MHz at 257.6 mT and 12.9 MHz at 301.8 mT) is due to $^1$H nuclei near to the $VO^{2+}$ ion (phthalocyanine protons and/or solvent protons). Because the HFC of $^1$H nuclei is not the subject of this paper, we do not consider the $^1$H signal here. Figures 2a and 2d exhibit intense peaks at 6.4 and 9.5 MHz. Since the separation of these peaks (3.1 MHz) agrees well with $4\nu(^{14}\mathrm{N})$ (=3.17 MHz at 257.6 mT), they are readily assigned to the DQ lines. Note that the actual separation can be slightly smaller than $4\nu(^{14}\mathrm{N})$, owing to higher order effects. In the present case, however, the difference between $4\nu(^{14}\mathrm{N})$ and the actual separation is small, which shows that the higher order effects

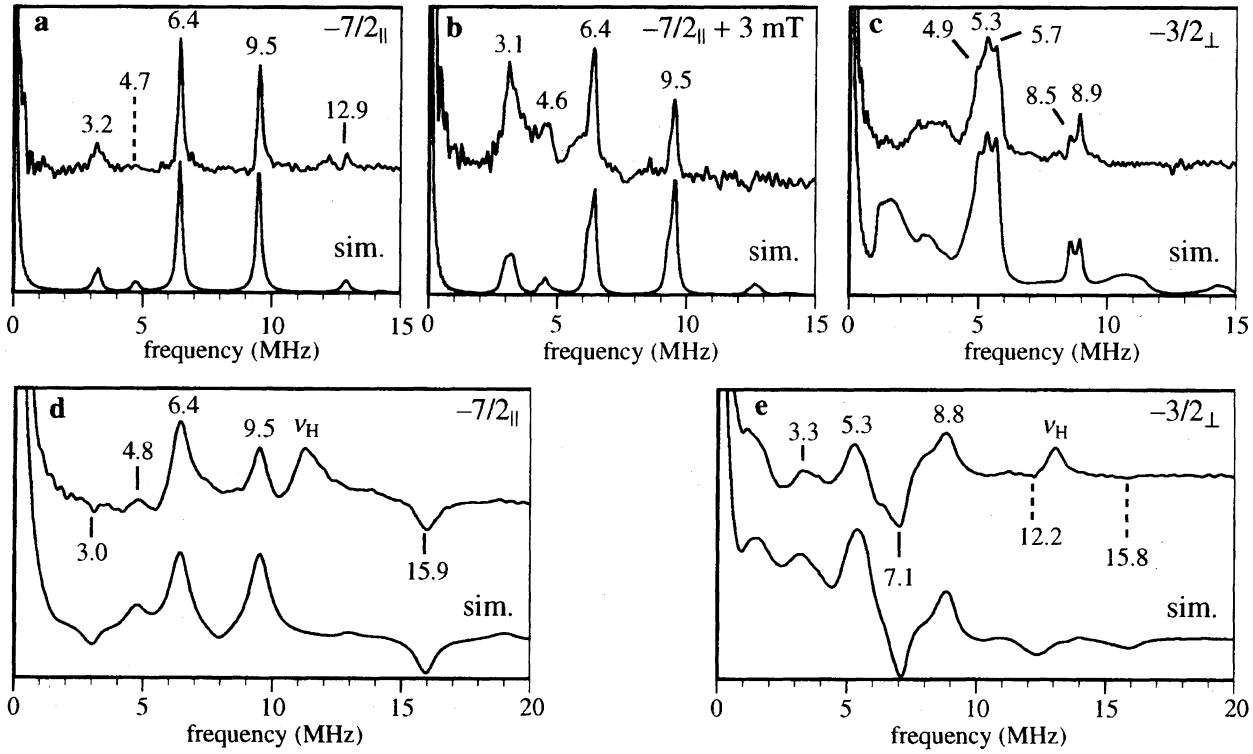


Fig. 2. Three-pulse (a, b, and c) and two-pulse (d and e) ESEEM spectra of [VO(tcpc)] in DMF/toluene (1 : 1 v/v) glass. Conditions: frequency, 8.708 GHz; temperature, 77 K; $B = 257.6$ mT (a), 260.7 mT (b), 301.8 mT (c), 257.6 mT (d), 301.8 mT (e); $\tau = 360$ ns (a), 360 ns (b), 310 ns (c). The lower trace in each panel represents the best fit to the experimental data. The peaks denoted with $\nu_H$ are due to $^1H$ nuclei.

are small and that Eqs. 1 and 2 can be safely used. Hence, the parallel component of HFC can be estimated using Eq. 1 as $|A_z| \approx 7.95$ MHz. Figures 2a and 2d also contain weak peaks at 3.2 and 4.8 MHz, respectively, which are attributed to the SQ lines. There are two choices for assigning these peaks: one choice is to assign the 3.2 MHz peak to $\nu_{sq-}{}^{(1)}$ (or $\nu_{sq-}{}^{(2)}$) and the 4.8 MHz peak to $\nu_{sq+}{}^{(1)}$ (or $\nu_{sq+}{}^{(2)}$); the other is to assign the 3.2 MHz peak to $\nu_{sq+}{}^{(2)}$ and the 4.8 MHz peak to $\nu_{sq-}{}^{(1)}$. Computer simulations executed individually for the two cases revealed that the former choice is appropriate, which leads to an estimate of $|Q_z| \approx 1.0$—1.1 MHz. Figure 2a also contains a very weak peak at 12.9 MHz. This peak frequency is in good accordance with two-times the peak frequency of the lower DQ line, i.e. $2\nu_{dq-}$. Thus, this peak is attributed to a multinuclear combination line. The negative peaks at 3.0 and 15.9 MHz in Fig. 2d are assigned to "sum and difference" combination lines $\nu_{dd-}$ and $\nu_{dd+}$, respectively, which are characteristic of two-pulse spectra.

The three-pulse spectrum recorded at "$-7/2_{\|}+3$ mT" (Fig. 2b) exhibits DQ lines at 6.4 and 9.5 MHz and SQ lines at 3.1 and 4.6 MHz. As noted above, the intensities of the SQ lines are greatly enhanced in the "$-7/2_{\|}+3$ mT" spectrum owing to the deviation of the applied field from the tensor axis, though the peak frequencies are not remarkably changed because the deviation is still not very large (ca. 20°). Another important change occurs in regard to the lineshape of the DQ line: in the "$-7/2_{\|}+3$ mT" spectrum, the DQ lines display a significantly asymmetric lineshape, where a shoulder-like feature is seen in the lower-frequency side (this may be more clearly seen in Fig. 3b). As described below, simulations show that this feature is due to a deviation of the nitrogen local $z$ axis from the $g_z$ axis.

The three-pulse spectrum recorded at "$-3/2_{\perp}$" (Fig. 2c) exhibits two peaks (8.5 and 8.9 MHz) in the region of the higher-frequency DQ line, which are assigned to the two perpendicular components ($x$ and $y$) of $\nu_{dq+}$. We label the smaller frequency component (8.5 MHz) as $x$ and the larger one (8.9 MHz) as $y$. At 301.8 mT, the first-order separation of the DQ lines is $4\nu(^{14}N) = 3.7$ MHz, so that the lower frequency partners of the 8.5 and 8.9 MHz peaks are assigned to the 4.9 and 5.3 MHz peaks, respectively. Thus, one can estimate $|A_x| \approx 6.7$ and $|A_y| \approx 7.1$ MHz using Eq. 1. The remaining peak at 5.7 MHz is most likely the high-frequency edge of the SQ line, which corresponds to the maximum-frequency SQ line in the $xy$ summation. The two-pulse spectrum recorded at this position (Fig. 2e) exhibits broad DQ lines at 5.3 and 8.8 MHz, where the $x$ and $y$ components are merged. Figure 2e also shows an intense negative peak at 7.1 MHz. This peak is attributed to a sum combination, $\nu_{ss+} = \nu_{sq\pm}{}^{(1)} + \nu_{sq\mp}{}^{(2)} \approx |A_\zeta|$. Quite interestingly, because of the small variation of $|A_\zeta|$ in the $xy$ summation (roughly $|A_x| \approx 6.7$—$|A_y| \approx 7.1$ MHz), this combination survives the $xy$ summation to exhibit an intense line, even though the parent SQ lines are broadened out.

Computer simulations were carried out using the above estimated HFC and NQC parameters as a first input. The

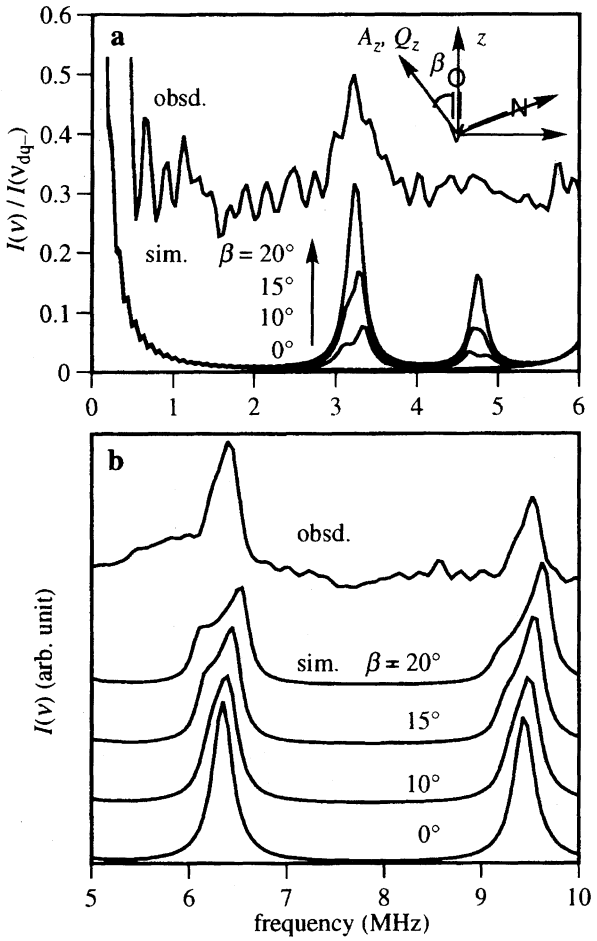


Fig. 3. Effects of the variation of the Euler angle $\beta$ on the intensities of the SQ lines in the three-pulse ESEEM spectrum recorded at "$-7/2_{||}$" (**a**) and on the lineshapes of the DQ lines in the spectrum recorded at "$-7/2+3$ mT" (**b**). The simulations were obtained with the other parameters fixed at the best-fit values of [VO(tcpc)] listed in Table 2. The experimental spectra in **a** and **b** are the enlargement of the spectra in Figs. 2a and 2b, respectively.

resulting best fits to the experimental spectra are included in Fig. 2, and the best-fit parameters are listed in Table 2. The best-fit values are not very different from their respective first input values, which confirms the above assignments of the peaks. As noted above, the weak SQ lines in the "$-7/2_{||}$" spectrum show that the $g_z$, $A_z$, and $Q_z$ axes can be regarded as roughly collinear. However, the fact that the SQ lines are still observable in the "$-7/2_{||}$" spectrum indicates that the deviation among the $g_z$, $A_z$, and $Q_z$ axes are not completely negligible. Simulations allowing a variation in the Euler angles showed that the variation of $\beta$ can greatly improve the fittings, whereas the variations of the other Euler angles are almost meaningless. The effects of $\beta$ are demonstrated in Fig. 3.[20] Figure 3a compares a series of computed spectra with the experimental three-pulse spectrum recorded at the $-7/2_{||}$ line, demonstrating the $\beta$ dependence of the SQ line intensities (each spectrum is normalized with the intensity of the $\nu_{dq-}$ line at 6.4 MHz). In the computed spectra, two bands of the SQ lines become visible at $\beta \neq 0°$, and gain more intensities as $\beta$ increases. One band appears in a region of 3.0—3.5 MHz. At $\beta = 15°$, its normalized intensity becomes ca. 0.2, becoming comparable to the intensity of the 3.2 MHz peak in the experimental spectrum. The other band appears in a range 4.5—5 MHz in the simulations. The computed intensity for this band is, however, weak even at $\beta = 15°$, so that this band is most likely obscured by noise in the experimental spectrum. Another conspicuous effect of $\beta$ is to distort the DQ lines in the "$-7/2_{||}+3$ mT" spectrum. Figure 3b demonstrates the change in the lineshapes of the DQ lines with the variation of $\beta$. As $\beta$ increases, the DQ lines become asymmetric with the lower frequency tails swelling into shoulders. A comparison between the series of computed spectra and the experimental spectrum shows that the best fit can also be achieved around $\beta = 15°$.

**ESEEM Spectroscopy, [VO(tbpc)].** Since the ESEEM spectra of [VO(tbpc)] were found to be very similar to those of [VO(tcpc)], we only depict the three-pulse spectra recorded at positions "$-7/2_{||}$" and "$-7/2_{||}+3$ mT" in Fig. 4. The HFC and NQC parameters estimated from the first-order equations for this complex were almost identical with those for [VO(tcpc)]. A subtle difference between the two complexes is that the SQ lines are not clearly resolved in the "$-7/2_{||}$" spectrum of [VO(tbpc)] (Fig. 4a). This may indicate a smaller deviation of the nitrogen local $z$ axis from the $g_z$ axis. Nevertheless, the asymmetric DQ lines in the "$-7/2_{||}+3$ mT" spectrum indicates that a deviation of the tensor axes still occurs in [VO(tbpc)] (Fig. 4b and its enlargement in Fig. 4c). The best fits to the experimental spectra

Table 2. $^{14}$N ESEEM Parameters of Oxovanadium(IV) Phthalocyanines and Oxovanadium(IV) Porphyrins

| | HFC/MHz[a] | | | | NQC/MHz[a] | | | Euler angle[a,b] |
|---|---|---|---|---|---|---|---|---|
| | $\|A_x\|$ | $\|A_y\|$ | $\|A_z\|$ | $\|A_{iso}\|$ | $Q_x$ | $Q_y$ | $Q_z$ | $\beta$/deg |
| [VO(tcpc)] | 6.50 | 7.00 | 7.75 | 7.08 | −1.10 | 1.00 | 0.10 | 15 |
| [VO(tbpc)] | 6.55 | 6.95 | 7.75 | 7.08 | −1.05 | 0.95 | 0.10 | 10 |
| [VO(tapc)] | 6.50 | 6.95 | 7.70 | 7.05 | −0.80 | 1.00 | −0.20 | 15 |
| [VO(oep)][c] | 6.7 | 7.2 | 7.7 | 7.2 | −0.75 | 1.0 | −0.25 | |
| [VO(tpp)][c] | 6.8 | 7.3 | 7.8 | 7.3 | −0.75 | 0.95 | −0.20 | |

a) Estimated uncertainties are ±0.1 for HFC and NQC parameters and ±5° for the Euler angle $\beta$. b) The other Euler angles are set at the ideal values; $\alpha = 0, 90, 180, 270°$ and $\gamma = 0°$. c) Taken from Ref. 7.

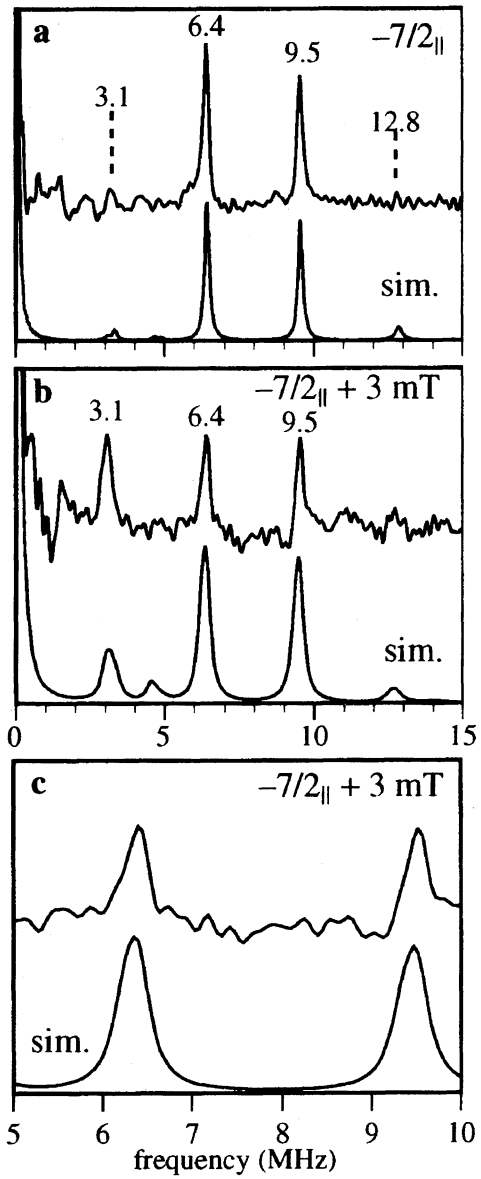


Fig. 4. Three-pulse ESEEM spectra of [VO(tbpc)] in DMF/toluene (1 : 1 v/v) glass. Conditions: frequency, 8.707 GHz; temperature, 77 K; $B$ = 257.5 mT (a), 260.5 mT (b); $\tau$ = 360 ns (a), 360 ns (b). The panel c is an enlargement of b. The lower trace in each panel represents the best fit to the experimental data.

were obtained with a slightly smaller Euler angle of $\beta = 10°$.

**ESEEM Spectroscopy, [VO(tapc)].** Figure 5 shows selected ESEEM spectra of [VO(tapc)]: the three-pulse spectra recorded at "$-7/2_{\|}$", "$-7/2_{\|}$+3 mT" and "$-3/2_{\perp}$", and two-pulse spectra recorded at "$-7/2_{\|}$" and "$-3/2_{\perp}$". These spectra are roughly similar to those of the above two complexes ([VO(tcpc)] and [VO(tbpc)]), and the assignments of the peaks and estimates of the HFC and NQC parameters can be made in the same manner as described above. Nevertheless, there are two remarkable differences in the ESEEM spectra between [VO(tapc)] and the other complexes. One is that the "$-7/2_{\|}$" spectrum of [VO(tapc)] does not exhibit SQ lines (Fig. 5a), although the asymmetric DQ lines in the "$-7/2$+3 mT" spectrum (Fig. 5b) still indicate a deviation of the nitrogen local $z$ axis from $g_z$. The other is that the intensity distribution between the $x$ and $y$ components of the DQ lines in the "$-3/2_{\perp}$" spectrum is altered. In Fig. 5c, we assign the 4.9 and 8.6 MHz peaks to the $x$ components of $\nu_{dq-}$ and $\nu_{dq+}$, respectively, and the 8.8 MHz peak to the $y$ component of $\nu_{dq+}$. The 5.8 MHz peak is assigned to the high-frequency edge of the SQ line, and the $y$ component of $\nu_{dq-}$ is most likely buried between the 4.9 and 5.8 MHz peaks. A comparison between the "$-3/2_{\perp}$" spectra of [VO(tapc)] and [VO(tcpc)] reveals that the $x$ components become relatively intense in the spectrum of [VO(tapc)]. The $x$ components (4.9 and 8.6 MHz peaks) in Fig. 5c are relatively intense compared with the 4.9 and 8.5 MHz peaks in Fig. 2c. The same change in the intensity distribution was found in the three-pulse spectra recorded at the "$1/2_{\perp}$" line (data not shown). Simulations showed that the intensity distribution for [VO(tapc)] can not be reproduced without taking the orientation of the NQC unique axis as being different from that in [VO(tcpc)] and [VO(tapc)].[21]

The best-fit parameters are listed in Table 2 as well. The resulting NQC unique axis for this complex is parallel to the axis containing the middle-magnitude HFC component ($A_y$). This is in contrast to the results that the unique axis for [VO(tcpc)] and [VO(tbpc)] is parallel to the axis containing the smallest-magnitude HFC component ($A_x$). The relation between the orientation of the NQC unique axis and the intensity distribution between the components of the DQ line will be considered in the Discussion section.

## Discussion

We have determined from computer simulations the principal values and the axis orientations of the HFC **A** and NQC **Q** tensors of the phthalocyanine isoindole nitrogens (Table 2). The resulting HFC parameters are very similar among the three complexes. Their isotropic HFC parameters are $|A_{iso}| = 7.05$—$7.08$, being fairly similar to the $|A_{iso}|$ values of oxovanadium(IV) porphyrins (7.2—7.3 MHz)[7] and distinctively larger than those of other $sp^2$-hybrid nitrogens (ca. 6—6.5 MHz).[3,5,6,22] Thus, with respect to the strength of HFC, the phthalocyanine isoindole nitrogen can be classified into the same subclass as the porphyrin pyrrole nitrogen. As for the NQC parameters, on the other hand, we have found a change in the unique-axis orientation, where the unique axis is parallel to the middle-magnitude HFC axis ($A_y$) in [VO(tapc)], whereas this axis is parallel to the smallest magnitude HFC axis ($A_x$) in [VO(tcpc)] and [VO(tbpc)]. Of the three, [VO(tapc)] possesses NQC very similar to that of the oxovanadium(IV) porphyrins.

The computer simulations have shown that the orientation of the NQC unique axis is closely related with the intensity distribution between the components of the DQ line. A theoretical explanation for this can be given as follows. As previously reported,[3,23] the intensity of the DQ $\zeta$ component ($I_\zeta$) is approximately proportional to $|Q_\xi - Q_\eta|^2/A_\zeta{}^2$, where $\xi$ and $\eta$ are the other NQC axes, provided that the relation HFC$\gg$NQC, NZC holds and the deviations of the tensor

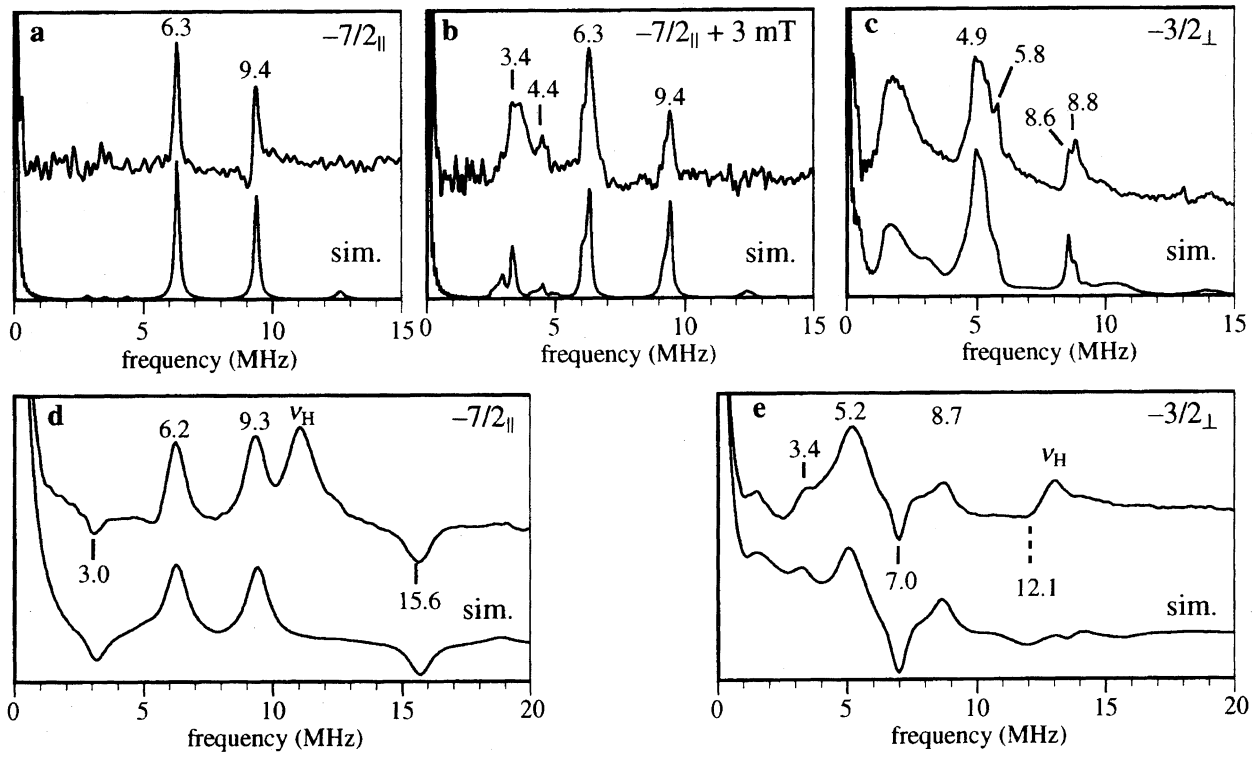


Fig. 5. Three-pulse (a, b, and c) and two-pulse (d and e) ESEEM spectra of [VO(tapc)] in DMF/toluene (1 : 1 v/v) glass. Conditions: frequency, 8.706 GHz; temperature, 77 K; $B$ = 256.7 mT (a), 259.7 mT (b), 301.3 mT (c), 256.7 mT (d), 301.3 mT (e); $\tau$ = 360 ns (a), 360 ns (b), 310 ns (c). The lower trace in each panel represents the best fit to the experimental data. The peaks denoted with $\nu_H$ are due to $^1$H nuclei.

axes are small. When HFC is quite isotropic as in the present case, one can include the factor $A_\xi{}^{-2}$ into a constant ($k$) and write as $I_\xi \approx k(Q_\xi - Q_\eta)^2$. Then, since the NQC tensor is traceless ($Q_z = -Q_x - Q_y$), the expected intensities for the DQ $x$ and $y$ components can be expressed as

$$I_x \approx k(Q_y - Q_z)^2 = k(Q_x + 2Q_y)^2, \quad (3a)$$

$$I_y \approx k(Q_x - Q_z)^2 = k(2Q_x + Q_y)^2, \quad (3b)$$

which provides

$$I_x - I_y \approx 3k(Q_y{}^2 - Q_x{}^2). \quad (3c)$$

This approximated equation predicts that the $x$ component should become intense in comparison with the $y$ component as $|Q_y|$ increases and, reversely, the $y$ component should become intense in comparison with the $x$ component as $|Q_x|$ increases. In other words, of the three cases where magnetic fields are respectively applied along the NQC principal axes, the magnetic field along the unique axis provides the weakest DQ lines. It is interesting to point out that the same field-orientation dependence of the DQ line intensity was reported concerning the remote nitrogen ESEEM signal of $Cu^{2+}$-imidazole complexes, where the exact cancellation occurs: HFC $\approx$ NZC.[24]

In addition, simulations showed that the change in the NQC unique-axis orientation causes a change in the intensities of the SQ lines in the "$-7/2_{\|}$" spectrum. It was found that, when $Q_y$ is set to the unique axis as in [VO(tapc)], the increase in $\beta$ from 0° does not effectively enhance the SQ line intensities. As can be seen in Fig. 5a, the simulated spectrum exhibits extremely weak SQ lines, even though it is computed with $\beta$ = 15°. This is in good contrast to the simulations in Fig. 3a, where $Q_x$ is set to the unique axis and the SQ lines are remarkably enhanced with the increase in $\beta$. This property of the SQ line intensity reasonably explains the absence of the SQ lines in the "$-7/2_{\|}$" spectrum of [VO(tapc)] in spite of the asymmetric DQ lines in the "$-7/2$+3 mT" spectrum.

During the simulations, we simply labeled the smaller magnitude in-plane HFC axis as $x$, and the remaining in-plane axis as $y$. Since the two in-plane axes are experimentally indistinguishable, the orientations of the nitrogen $x$ and $y$ axes with respect to the nitrogen local geometry can not be determined only from simulations. In fact, simulations provide the same spectrum when $A_x$ and $A_y$, and $Q_x$ and $Q_y$ are simultaneously interchanged. (Then the Euler angles must be also changed as, for example, $\alpha, \beta, \gamma = 0°, 15°, 0°$ to $90°, 15°, 90°$.) Determining the orientations of the nitrogen $x$ and $y$ axes, therefore, requires consideration of the mechanism of HFC. The HFC of nitrogen nuclei coordinating to the $VO^{2+}$ ion has been studied for several types of nitrogens, and it is now believed that their HFC arises predominantly from indirect spin transfer of the vanadium unpaired electron spin to the nitrogen lone-pair orbital.[3] The indirect spin transfer produces a negative spin population on the nitrogen orbital, and thus the HFC principal values should be negative.[25]

Furthermore, the HFC tensor will be quite isotropic, because the lone-pair orbital contains a sufficient s-orbital character (25—50%, depending on its $sp^n$ hybridization ratio) and the s-orbital electron interacts with the nuclear spin much stronger than does the p-orbital electron. The through-space dipole–dipole interaction is believed to provide a minor contribution, rendering HFC slightly uniaxial with respect to the V–N bond axis. Since the HFC component along the V–N bond axis due to the dipole–dipole interaction is positive, this component will be the largest of the three principal components. Since the signs of the HFC components are expected to be negative, the component along the V–N bond axis should consequently be the smallest in magnitude. We have chosen $|A_x|$ as being smaller than $|A_y|$, and Table 2 shows that $|A_x|$ is also always smaller than $|A_z|$. Therefore we conclude that this $A_x$ axis is parallel to the V–N bond.

Equations for the HFC parameters based on the above mechanism have been given previously.[3] In the previous equations, it is assumed that HFC is axial with respect to the V–N bond. For the oxovanadium(IV) phthalocyanines, however, the rhombicity of HFC is found to be relatively large compared with the rhombicity for other $VO^{2+}$ complexes. It was pointed out that the rhombicity of HFC predominantly arises from an additional negative polarization of the nitrogen π orbital.[3] Thus, the literature equations can be modified to include the rhombicity, as:

$$A_x = \rho_n c_s^2 A_0(\mathrm{N2s}) + (2\rho_n c_p^{\,2} - \rho_\pi) A_0(\mathrm{N2p}) + 2A_{dd}, \quad (4a)$$

$$A_y = \rho_n c_s^2 A_0(\mathrm{N2s}) - (\rho_n c_p^{\,2} + \rho_\pi) A_0(\mathrm{N2p}) - A_{dd}, \quad (4b)$$

$$A_z = \rho_n c_s^2 A_0(\mathrm{N2s}) - (\rho_n c_p^{\,2} - 2\rho_\pi) A_0(\mathrm{N2p}) - A_{dd}. \quad (4c)$$

The HFC parameters for the unit unpaired electron on the nitrogen 2s and 2p orbitals are denoted as $A_0(\mathrm{N2s}) = 1811$ and $A_0(\mathrm{N2p}) = 55.5$ MHz, respectively.[26] The symbols $\rho_n$ and $\rho_\pi$ are the spin populations of the nitrogen lone-pair and π orbitals, respectively (Fig. 6), and $c_s$ and $c_p$ are the coefficients of the 2s and 2p orbitals, respectively, in the $sp^2$-hybrid lone-pair orbital (they satisfy $c_s^2 + c_p^2 = 1$). We use the values for normal $sp^2$ hybridization: $c_s = \sqrt{(1/3)}$ and $c_p = \sqrt{(2/3)}$.[27] The symbol $A_{dd}$ denotes the contribution from the dipole–dipole interaction, and can be expressed on the basis of the point-dipole approximation as

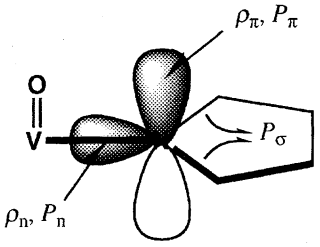


Fig. 6. Schematic drawing of the $sp^2$-hybrid nitrogen orbitals.

$$A_{dd} = \frac{\mu_0}{4\pi} \frac{g_e \mu_B g(^{14}\mathrm{N}) \mu_N}{hr^3}, \quad (5)$$

where $r$ is the V–N bond length and the other symbols have their usual meanings. By using Eqs. 4 and 5, one can estimate the spin populations ($\rho_n$ and $\rho_\pi$) and the V–N bond length ($r$) from the HFC parameters ($A_x$, $A_y$, and $A_z$). Assigning the smallest-magnitude component to $A_x$ and the remaining in-plane component to $A_y$, one obtains V–N bond lengths of 2.12—2.16 Å (Table 3). These values can be compared with the X-ray determined bond length of 2.026 Å for [VO(pc)].[28] On the other hand, when $A_x$ and $A_y$ are interchanged, one calculates V–N bond lengths that are too large, as typically shown for the case of [VO(tapc)] in Table 3. These results confirm the assignment of the smallest magnitude HFC axis to the V–N bond axis.

The conclusion that the smallest-magnitude HFC axis is invariably parallel to the V–N bond means that the NQC unique axis is parallel to the V–N bond for [VO(tcpc)] and [VO(tbpc)], whereas it is perpendicular to the V–N bond for [VO(tapc)]. We show in the following that such a change in the orientation of the NQC unique axis is not surprising. According to the Townes–Dailey model[29] developed by Brown et al.,[30] the NQC principal components of the $sp^2$-hybrid nitrogen can be expressed in terms of the electron populations of the nitrogen lone-pair orbital, σ orbitals, and π orbital (denoted as $P_n$, $P_\sigma$, and $P_\pi$, respectively, as illustrated in

Table 3. Spin Populations $\rho_\chi$ and Electron Populations $P_\chi$ of the Nitrogen Orbitals ($\chi$ = σ, n, π) Estimated from the $^{14}$N HFC and NQC Parameters

| | HFC[a] | | | | | NQC[b] | | |
|---|---|---|---|---|---|---|---|---|
| | $c_s$[c] | $\rho_n$/% | $\rho_\pi$/% | $r$/Å | $r_{X\text{-ray}}$/Å | $P_\sigma$[c] | $P_n$ | $P_\pi$ |
| [VO(tcpc)] | $\sqrt{(1/3)}$ | −1.17 | −0.45 | 2.12 | 2.026 | 1.28 | 1.75 | 1.41 |
| [VO(tbpc)] | $\sqrt{(1/3)}$ | −1.17 | −0.48 | 2.16 | | 1.28 | 1.72 | 1.41 |
| [VO(tapc)] | $\sqrt{(1/3)}$ | −1.17 | −0.45 | 2.14 | | 1.28 | 1.68 | 1.46 |
| | $\sqrt{(1/3)}$ | −1.17 | −0.72 | 2.72 | ($A_x$ and $A_y$ interchanged) | | | |
| [VO(oep)][d] | $\sqrt{(1/3)}$ | −1.19 | −0.30 | 2.11 | 2.102 | 1.28 | 1.67 | 1.47 |
| [VO(tpp)][d] | $\sqrt{(1/3)}$ | −1.21 | −0.30 | 2.10 | 2.080 | 1.28 | 1.66 | 1.45 |

a) The uncertainties originating from the uncertainties of the HFC parameters are ca. ±0.01%, ±0.09%, and ±0.06 Å for $\rho_n$, $\rho_\pi$, and $r$, respectively. b) The uncertainties originating from the uncertainties of the NQC parameters are ca. ±0.03 and ±0.02 for $P_n$ and $P_\pi$, respectively. c) Fixed parameter. d) Taken from Ref. 7.

Fig. 6) as

$$Q_x = Q_0[(1 - c_s^2)(P_n - P_\sigma) - (1/2)(P_\pi - P_\sigma)], \quad (6a)$$

$$Q_y = Q_0[-(1/2)(1 - c_s^2)(P_n - P_\sigma) - (1/2)(P_\pi - P_\sigma)], \quad (6b)$$

$$Q_z = Q_0[-(1/2)(1 - c_s^2)(P_n - P_\sigma) + (P_\pi - P_\sigma)], \quad (6c)$$

where $Q_0$ is a constant, $Q_0 = -4.5$ MHz. Equation 6 can be rewritten into

$$P_n - P_\sigma = 2(Q_x - Q_y)/[3Q_0(1 - c_s^2)]. \quad (7a)$$

$$P_\pi - P_\sigma = 2(Q_z - Q_y)/(3Q_0). \quad (7b)$$

which show that the electron populations $P_n$ and $P_\pi$ can be estimated as a difference from $P_\sigma$. By again setting $c_s = \sqrt{(1/3)}$, one obtains, for example, $P_n - P_\sigma = 0.47$ and $P_\pi - P_\sigma = 0.13$ for [VO(tcpc)]. It would, however, be more instructive to provide definite values for $P_n$ and $P_\pi$, which requires an estimate of $P_\sigma$. Fortunately, the electron population of the σ orbital is expected to be fairly unaffected by the substituents, so that $P_\sigma$ may be regarded as being constant. Here, we use $P_\sigma = 1.28$ on the basis of previous density functional calculations, which yielded a total charge of $-0.6888$ ($= 5 - 2P_\sigma - P_n - P_\pi$) for the isoindole nitrogen of Co(pc).[31] The charge of the nitrogen in [VO(pc)] would not be extremely different from this value (unfortunately, it seems that corresponding calculations have not been made for [VO(pc)]). The value $P_\sigma = 1.28$ is slightly larger than 1.0, being consistent with the fact that nitrogen has a slightly larger electron affinity than does the carbon. Table 3 summarizes the $P_n$ and $P_\pi$ values of the oxovanadium(IV) phthalocyanines and porphyrins calculated using this $P_\sigma$ value. In a naïve scheme, $P_n$ would be 2.0 (no donation to the vanadium) and $P_\pi$ would be 1.5 (the average of the values for the N and $N^-$ valence states). In reality, donation of the lone-pair electrons to vanadium and spread of the $N^-$ electrons over the phthalocyanine π system will reduce $P_n$ and $P_\pi$, respectively, from these naïve values. The resulting $P_n$ and $P_\pi$ values are therefore quite reasonable. It is important to note that the $P_n$ and $P_\pi$ values fall in small ranges (1.66—1.75 and 1.41—1.47, respectively) in spite of the difference in the unique-axis direction among them. This demonstrates that even such a small change of the electron populations can induce a change in the NQC unique-axis orientation.

Table 3 suggests that the $P_\pi$ values of the phthalocyanines are generally smaller than those of the porphyrins. This presumably reflects the fact that the averaged number of π electrons per one atom is smaller in the phthalocyaninate dianion (1.05 π electrons per one atom, 42 π electrons over 40 atoms) than in the porphyrinate dianion (1.08 π electrons per atom, 26 π electrons over 24 atoms). A close inspection of Table 3 also reveals that the $P_\pi$ value of [VO(tapc)] is subtly larger than those of [VO(tcpc)] and [VO(tbpc)]. This is in agreement with the expectation that the amine substituent would increase the electron population of the phthalocyanine π orbital due to conjugation with the amine lone-pair orbital. This increase of $P_\pi$ seems to be the main reason for the change of the NQC unique-axis orientation. As for [VO(tcpc)], on the other hand, one may expect a decrease of $P_\pi$ due to substituent effects of the carboxyl group. The calculation, however, yielded no difference between the $P_\pi$ values of [VO(tcpc)] and [VO(tbpc)]. This may indicate that the carboxyl group mainly withdraws electrons from carbon atoms, not from nitrogen atoms, owing to the difference in electron affinity between the two atoms. A meaningful variation is also found in the electron population of the lone-pair orbital $P_n$. The $P_n$ value of [VO(tapc)] is slightly smaller than those of [VO(tcpc)] and [VO(tbpc)]. This difference can be attributed to the induction effect,[30] where the electron population of the lone-pair orbital is decreased with an increase of the π-orbital electron population because of the Coulomb repulsion between them. (Unfortunately the difference between the $P_n$ values of [VO(tcpc)] and [VO(tbpc)] is not larger than the uncertainty.)

We have concluded from the simulations that the HFC and NQC $x$ and $z$ axes are considerably deviated from the $g_\perp$ plane (the phthalocyanine plane) and the $g_\parallel$ axes (the V=O bond axis), respectively, with the deviation angle being $\beta = 10$—$15°$. Since the HFC and NQC $x$ axis should coincide with the V–N bond axis, these results suggest a molecular geometry where the V–N bonds are tilted from the phthalocyanine plane by $\beta \approx 10$—$15°$. X-Ray data of [VO(pc)] shows that the vanadium atom is situated above the phthalocyanine plane, and that the distance between the vanadium atom and the four nitrogen plane is 0.575 Å and the mean V–N bond length is 2.026 Å.[28] Hence, in the crystalline state, the angle between the V–N bond and the phthalocyanine plane is $\sin^{-1}(0.575/2.026) = 16.5°$. This value is very close to $\beta = 10$—$15°$ determined from the simulations, which can be strong support for the simulations. Furthermore, this agreement suggests that the oxovanadium(IV) phthalocyanines do not receive such strong solvent coordination as to cause a movement of the vanadium atom into the phthalocyanine plane in DMF/toluene glass.

In summary, we have described the ESEEM results of the three oxovanadium(IV) phthalocyanines. The HFC tensors of the phthalocyanines have been found to be almost identical with one another, and, furthermore, quite similar to those of oxovanadium(IV) porphyrins. In contrast, a remarkable difference has been found between the NQC tensors. The unique axis is along the V–N bond in [VO(tcpc)] and [VO(tbpc)], whereas this is perpendicular to the V–N bond within the phthalocyanine plane in [VO(tapc)]. Quite interestingly, the NQC tensor of [VO(tapc)] is exceptionally similar to those of the oxovanadium(IV) porphyrins. An analysis of NQC based on the Townes–Dailey model indicates that the occurrence of the different unique-axis orientation in [VO(tapc)] is due to an increase of the nitrogen π-orbital electron population induced by the electron- donating amino group.

## References

1) For example: W. B. Mims and J. Peisach, in "Advanced EPR. Applications in Biology and Biochemistry," ed by A. J. Hoff,

Elsevier, Amsterdam (1989).

2) S. A. Dikanov and A. V. Astashkin, in "Advanced EPR. Applications in Biology and Biochemistry," ed by A. J. Hoff, Elsevier, Amsterdam (1989).

3) K. Fukui, H. Ohya-Nishiguchi, and H. Kamada, *Inorg. Chem.*, **36**, 5518 (1997), and references cited therein.

4) A few exceptions to this correlation rule may be found in Ref. 5 and the following: B. J. Hamstra, A. L. P. Houseman, G. J. Colpas, J. W. Kampf, R. LoBrutto, W. D. Frasch, and V. L. Pecoraro, *Inorg. Chem.*, **36**, 4866 (1997).

5) a) E. J. Reijerse, J. Shane, E. de Boer, and D. Collison, in "Electron Magnetic Resonance of Disordered Systems," ed by N. D. Yordanov, World Scientific, Singapore (1989); b) E. J. Reijerse, J. Shane, E. de Boer, P. Höfer, and D. Collison, in "Electron Magnetic Resonance of Disordered Systems," ed by N. D. Yordanov, World Scientific, Singapore (1991).

6) K. Fukui, H. Ohya-Nishiguchi, and H. Kamada, *Inorg. Chem.*, **37**, 2326 (1998).

7) K. Fukui, H. Ohya-Nishiguchi, and H. Kamada, *J. Phys. Chem.*, **97**, 11858 (1993).

8) P. Kivits, R. de Bont, and J. van der Veen, *Appl. Phys.*, **A26**, 101 (1981).

9) K. Kasaga, M. Terauchi, M. Hara, K. Nishie, T. Sugimori, and M. Handa, *Bull. Chem. Soc. Jpn.*, **70**, 2107 (1997).

10) J. A. Thompson, K. Murata, D. C. Miller, J. L. Stanton, W. E. Broderick, B. M. Hoffman, and J. A. Ibers, *Inorg. Chem.*, **32**, 3546 (1993).

11) K.-Y. Lee, *Inorg. Chem.*, **24**, 1778 (1985).

12) N. Kobayashi, R. Higashi, and T. Tomura, *Bull. Chem. Soc. Jpn.*, **70**, 2693 (1987).

13) M. Abkowity and A. R. Monahhan, *J. Chem. Phys.*, **58**, 2281 (1973).

14) Y. Xu and S. Shi, *Appl. Magn. Reson.*, **11**, 1 (1996).

15) a) H. Barkhuijsen, R. de Beer, W. M. M. J. Bovée, and D. van Ormondt, *J. Magn. Reson.*, **61**, 465 (1985); b) R. de Beer and D. van Ormondt, in "Advanced EPR. Applications in Biology and Biochemistry," ed by A. J. Hoff, Elsevier, Amsterdam (1989).

16) a) W. B. Mims, *Phys. Rev. B*, **5**, 2409 (1972); b) W. B. Mims, *Phys. Rev. B*, **6**, 3543 (1972).

17) S. A. Dikanov, A. M. Tyryshkin, J. Hüttermann, R. Bogumil, and H. Witzel, *J. Am. Chem. Soc.*, **117**, 4976 (1995).

18) H. Flanagan and D. J. Singel, *J. Chem. Phys.*, **87**, 5606 (1987).

19) E. J. Reijerse, N. A. J. M. van Aerle, and C. P. Keijzers, *J. Magn. Reson.*, **67**, 114 (1986).

20) We performed further simulations allowing the misalignment between the nitrogen **A** and **Q** tensor axes. Although these simulations did not bring any meaningful improvements of the fittings, they showed that (1) the SQ line intensities in the "$-7/2_{||}$" spectrum depend essentially on the orientation of the **Q** tensor, not on the orientation of the **A** tensor; and that (2) the lineshapes of the DQ lines in the "$-7/2_{||}+3$ mT" spectrum depend essentially on the orientation of the **A** tensor, not on the orientation of the **Q** tensor. Hence, it would be possible to determine the orientations of the **A** and **Q** tensors separately if the experimental data had much better S/N, though the misalignment between the two tensor axes should be small, if any.

21) In the simulated spectrum of Fig. 5c, the $\nu_{dq+}$ $x$ line (8.6 MHz peak) is much more intense than the $\nu_{dq+}$ $y$ line (8.8 MHz peak). In this regard, one may feel that the agreement between the experimental and simulated spectra is not good. However, we suppose that this disagreement is rather due to some errors of the dead-time data reconstruction. It seems that the phase of the 8.6 MHz peak is wrongly reconstructed, and that the height of this peak is underestimated in the experimental spectrum. Similarly, in Fig. 2c, it seems that the 8.5 MHz peak in the experimental spectrum has a wrong phase and its height is underestimated. It is unfortunately difficult to reconstruct the dead-time data entirely correctly. Nevertheless, we evaluated the quality of fitting from the fit to the time-domain raw data, so that the results of the simulation are free from this problem.

22) A. V. Astashkin, S. A. Dikanov, and Y. D. Tsvetkov, *J. Struct. Chem.*, **26**, 363 (1985).

23) H. L. Flanagan and D. J. Singel, *J. Chem. Phys.*, **89**, 2585 (1988).

24) Y. Ohba, Y. Yoshida, and M. Iwaizumi, *Appl. Magn. Reson.*, **6**, 107 (1994).

25) C. P. Scholes, K. M. Falkoiwski, S. Chen, and J. Bank, *J. Am. Chem. Soc.*, **108**, 1660 (1986).

26) N. M. Atherton, in "Principles of Electron Spin Resonance," Ellis Horwood, New York (1993), pp. 87 and 197.

27) One may suppose that the s-orbital ratio should be taken as $c_s = 0.727$ for five-membered ring nitrogens such as the phthalocyanine isoindole nitrogens and porphyrin pyrrole nitrogens [T. G. Brown and B. M. Hoffman, *Mol. Phys.*, **39**, 1073 (1980)]. As pointed out previously,[3] however, this $c_s$ value provides an unreasonably long V–N bond length: For example, $r = 2.55$ Å is obtained for [VO(tapc)] with this $c_s$ value. When $A_x$ and $A_y$ are interchanged, the bond length becomes by far more unreasonable as $r = 5.09$ Å.

28) R. F. Ziolo, C. H. Griffiths, and J. M. Troup, *J. Chem. Soc., Dalton Trans.*, **11**, 2300 (1980).

29) C. H. Townes and D. B. Dailey, *J. Chem. Phys.*, **17**, 782 (1949).

30) a) Y.-N. Hsieh, G. V. Rubenacker, C. P. Cheng, and T. L. Brown, *J. Am. Chem. Soc.*, **99**, 1384 (1977); b) C. I. H. Ashby, C. P. Cheng, and T. L. Brown, *J. Am. Chem. Soc.*, **100**, 6057 (1978).

31) A. Rosa and E. J. Baerends, *Inorg. Chem.*, **33**, 584 (1994).